Journal of Materials Chemistry

www.rsc.org/materials

Volume 21 | Number 10 | 14 March 2011 | Pages 3253–3496

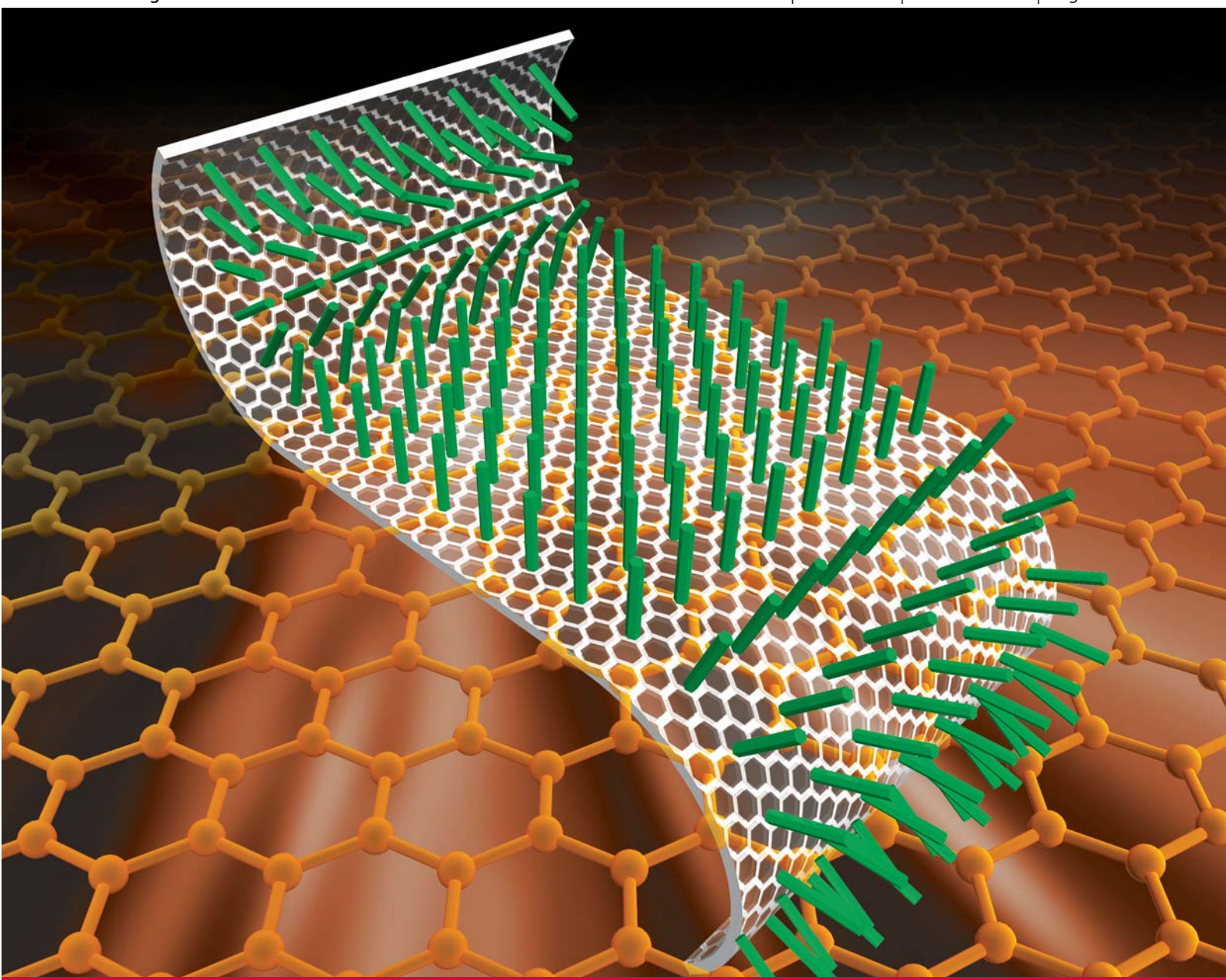

Graphene and carbon nanomaterials

ISSN 0959-9428

RSC Publishing

PAPER

J. O. Hwang *et al.*

Vertical ZnO nanowires/graphene hybrids for transparent and flexible field emission

International Year of CHEMISTRY 2011

0959-9428(2011)21:10;1-Q

Vertical ZnO nanowires/graphene hybrids for transparent and flexible field emission†‡

Jin Ok Hwang, Duck Hyun Lee, Ju Young Kim, Tae Hee Han, Bong Hoon Kim, Moonkyu Park, Kwangsoo No and Sang Ouk Kim*

Received 18th May 2010, Accepted 10th June 2010
DOI: 10.1039/c0jm01495h

We present a transparent and flexible optoelectronic material composed of vertically aligned ZnO NWs grown on reduced graphene/PDMS substrates. Large-area reduced graphene films were prepared on PDMS substrates by chemical exfoliation from natural graphite *via* oxidative aqueous dispersion and subsequent thermal reduction. ZnO NWs were hydrothermally grown on the reduced graphene film substrate and maintained their structural uniformity even in highly deformed states. The electrical contact between semiconducting ZnO NWs and the metallic graphene film was straightforwardly measured by electric force microscopy (EFM). It shows a typical metal–semiconductor ohmic contact without a contact barrier. Owing to the mechanical flexibility, transparency, and low contact barrier, the ZnO NWs/graphene hybrids show excellent field emission properties. Low turn-on field values of 2.0 V μm^{-1}, 2.4 V μm^{-1}, and 2.8 V μm^{-1} were measured for convex, flat, and concave deformations, respectively. Such variation of field emission properties were attributed to the modification of ZnO NWs emitter density upon mechanical deformation.

Introduction

ZnO nanowires (NWs) are transparent, wide band-gap semiconductor nanomaterials, potentially useful for electronics and optoelectronics.[1,2] In particular, vertical ZnO NWs are promising field emitters,[3–6] owing to their large shape anisotropy, and great thermal/chemical stability under oxygen environments. For such devices, vertical ZnO NWs have been produced either by catalytic gas phase syntheses,[7,8] or by solution phase syntheses.[9,10] In particular, hydrothermal solution phase synthesis ensure process scalability and cost efficiency, such that highly dense, catalyst-free, vertical ZnO NWs are readily grown, even below 100 °C under atmospheric pressure. Meanwhile, despite such attractive properties and facile processing, the substrate materials for vertical ZnO growth have been mostly limited to hard, flat substrate materials, such as indium tin oxide (ITO) and fluorine-doped tin oxide (FTO), thus far. Accordingly, the integration of vertical ZnO NWs in a flexible device remains a technological challenge.

Graphene is an emerging carbon material consisting of monolayered sp^2 hybrid carbon atoms.[11,12] Its atomic thickness and two-dimensional conjugated chemical structure cause a broad spectrum of attractive properties, such as optical transparency,[13] high electro-conductivity,[11] mechanical flexibility,[13,14] and strong thermal/chemical stability.[15–18] Such a synergistic combination of attractive properties renders graphene a promising component for next-generation flexible electronics and optoelectronics.

Department of Materials Science and Engineering, KAIST, Daejon, 305-701, Republic of Korea. E-mail: sangouk.kim@kaist.ac.kr; Fax: 82-42-350-3310; Tel: 82-42-350-3339

† This paper is part of a *Journal of Materials Chemistry* themed issue on Chemically Modified Graphenes. Guest editor: Rod Ruoff.

‡ Electronic supplementary information (ESI) available: Plane-view and cross-sectional SEM images of the reduced graphene film. Sheet resistance data of the reduced graphene film with 4-point probe. See DOI: 10.1039/c0jm01495h

Since the unexpected isolation of graphene by micromechanical drawing,[19] numerous approaches have been exploited for the large scale production of graphene.[20–26] Among them, chemical exfoliation of natural graphite *via* oxidative aqueous dispersion, namely the 'Hummers method'[27] and subsequent reduction, has proven to be a highly efficient and scalable process. In this approach, the aqueous dispersibility of the graphene oxide precursor facilitates the solution processing of natural graphite into highly uniform macroscopic graphene films or sheets that are mechanically flexible, electrically conductive, as well as optically transparent.

In this work, we introduce all-transparent ZnO NWs/graphene hybrids consisting of ZnO NWs vertically grown on reduced graphene film. Highly uniform, nanometre-scale thick, large-area reduced graphene films were prepared on a silicon substrate by spin casting from an aqueous dispersion and subsequent thermal reduction. The large-area reduced graphene film was transferred onto a flexible PDMS substrate to constitute a mechanically flexible/stretchable, electro-conductive, and optically transparent substrate. Hydrothermal synthesis[9,10,29] was employed to grow vertical ZnO NWs on the flexible substrate. The resultant ZnO NWs/graphene hybrid architecture maintained its structural integrity, even in a highly deformed state, and ohmic electrical contact through the semiconductor NWs and metallic graphene substrate junctions. As examples among many potential applications, the ZnO NW/graphene hybrids were readily integrated into a field-emitting device, whose remarkable performance under mechanical deformation is reported.

Experimental

Materials

Graphite was purchased from GK (product MGR 25 998 K), ethanol from J. T. Baker and hydrofluoric acid from DC

Chemical Corporation. PDMS (SYLGARD 184 Silicone Elastomer KIT) was purchased from Dow Corning Corporation. Zinc acetate dihydrate, zinc nitrate hexahydrate, and hexamethylenetetramine were purchased from Sigma-Aldrich.

Preparation of reduced graphene/PDMS substrates

Graphite oxide was prepared from a natural graphite by a modified Hummers method.[28] A fully exfoliated graphene oxide aqueous dispersion was achieved after sonication for 2 h and subsequent dialysis for 3 days. The resulting graphene oxide aqueous solution (0.3 wt%, 10 ml) was mixed with 10 ml of ethanol for spin casting. A graphene oxide film was spin cast upon a SiO_2 (500 nm)/Si substrate and thermally reduced at 600 °C for 30 min under a 100 sccm H_2 gas flow. The reduced graphene film was transferred onto a PDMS film thermally cured at 90 °C for several hours. Finally, the flexible reduced graphene film/PDMS substrate was prepared by peeling off from the silicon substrate in HF solution.

Synthesis of ZnO NWs/graphene hybrids

10 mM of ZnO seed solution (Zinc acetate dihydrate) in ethanol was spin cast on the reduced graphene/PDMS substrate. ZnO NWs were grown in an aqueous solution of 25 mM of zinc nitrate hexahydrate and 25 mM of hexamethylenetetramine at 90 °C for 3 h.

Characterization of ZnO NWs/graphene hybrids

The morphology and thickness of reduced graphene and ZnO NWs were characterized with a field emission scanning electron microscope (FESEM; Hitachi S-4800 SEM, Japan). The lattice structure and composition elements of ZnO NWs were characterized using a high-resolution transmission electron microscope (HRTEM; Philips Tecnai G2 F30) and energy dispersive spectrometer (TEM-EDS; Philips Tecnai G2 F30). Transmittance spectra of PDMS film, reduced graphene/PDMS substrate, and ZnO NWs/reduced graphene/PDMS hybrids were characterized by UV-vis spectroscopy (JASCO, V530, Japan).

Energy level measurements of the reduced graphene and ZnO NWs

The work function of metallic graphene and the work function and valence band of semiconducting ZnO NWs were obtained from ultraviolet photoelectron spectroscopy (UPS; AXIS-NOVA, Kratos Inc.). The band gap of the ZnO NWs was measured using a UV-vis spectrometer (JASCO, V530, Japan).

Sheet resistance of reduced graphene and electric current through single NW–graphene film junction measurements

The sheet resistance of reduced graphene was measured by 4-point probe equipment (CMT-SR1000N, AIT, Republic of Korea). The electrical characterization between reduced graphene and single ZnO NWs was measured in contact mode EFM (Seiko, N3800, Japan).

Fabrication of the reduced graphene transistor

Electron beam lithography was used to fabricate the Pd source and drain electrodes (thickness: 80 nm) in a field effect transistor test, with the boron-doped (p-type) silicon substrate (SiO_2 thickness of 500 nm) utilized as a back gate.

Field emission measurements

Flexible poly(ethylene terephthalate) (PET) films sputtered with 5 nm Au were utilized as the anode for the unbent or bent ZnO NWs/graphene hybrid cathodes. The spacing between the anode and the cathode was maintained at 200 μm. The field emitting properties were measured under a vacuum of $\sim 10^{-6}$ torr by applying a voltage of 0–3000 V between the two electrodes.

Results and discussion

The synthetic procedure for the production of ZnO NWs/graphene hybrids is schematically shown in Fig. 1. An aqueous dispersion of graphene oxide was prepared by a modified Hummers method.[28] Thin graphene oxide films were spin cast on SiO_2 (500 nm)/Si substrates from the aqueous dispersion. After thermal reduction at 600 °C for 30 min under a stream of H_2 gas, ~10 nm thick reduced graphene film was produced (ESI Fig. S1‡). The electro-conductivity of the reduced graphene film was ~20 kΩ/□ (ESI, Table S1‡). A PDMS film, thermally cured at 90 °C was put on the reduced graphene film. While the underlying SiO_2 was chemically etched in HF solution, the PDMS film tightly bound to reduced graphene film was quickly peeled off (Fig. 2a) and thoroughly washed with deionized water. After drying, the mechanically flexible, electro-conductive, transparent reduced graphene/PDMS substrate was prepared (Fig. 2b and c). Vertical ZnO NWs were grown from the graphene substrate following a two step hydrothermal synthesis. Firstly, ZnO seed solution (10 mM zinc acetate dihydrate in ethanol) was spin cast on the reduced graphene surface several times. After each spin casting, the seed layer was dried at 90 °C.

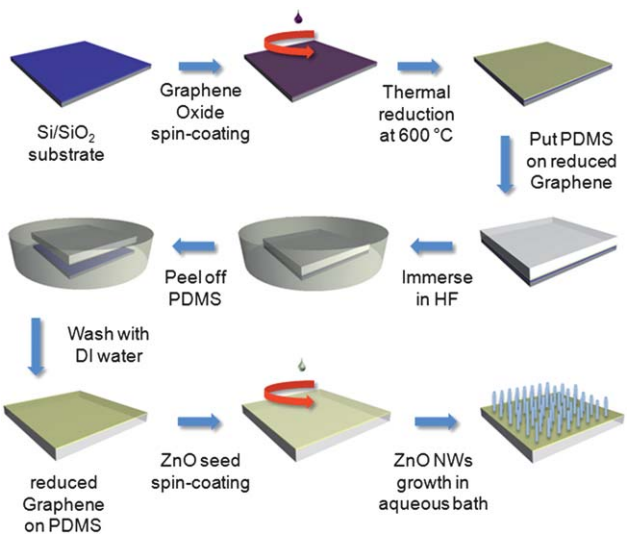

Fig. 1 A schematic illustration of the fabrication process of a transparent and flexible electrode composed of ZnO nanowires vertically grown on reduced graphene film/PDMS substrates.

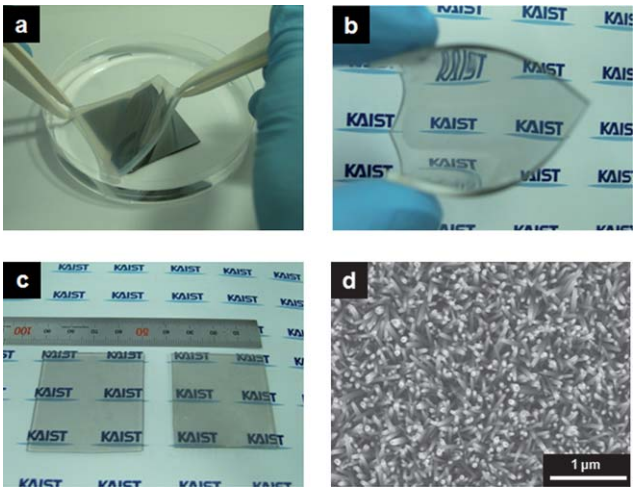

Fig. 2 Photographs and a SEM image demonstrating: (a) reduced graphene film transfer to PDMS in HF solution. (b) The flexibility and transparency of a reduced graphene/PDMS substrate. (c) Reduced graphene film/PDMS substrates (left) before and (right) after ZnO NWs growth, respectively. (d) A representative FE-SEM image of ZnO NWs vertically grown on the reduced graphene/PDMS substrate.

In the second step, ZnO NWs were grown by suspending the seeded graphene/PDMS substrate in an aqueous solution of zinc nitrate hexahydrate (25 mM) and hexamethylenetetramine (25 mM) at 90 °C for 3 h. The seeded graphene film side was face down during the NW growth to prevent precipitation of floating ZnO crystals on the substrate. Fig. 2c shows a photograph that compares reduced graphene/PDMS substrate before (left) and after (right) ZnO NW growth. Fig. 2d shows a plane view field-emission scanning electron microscopy (FE-SEM) image of the highly aligned, vertical ZnO NW arrays grown on a reduced graphene/PDMS substrate.

Fig. 3a shows a 60° tilted cross-sectional FE-SEM image of a ZnO NWs/graphene hybrid. ZnO NWs with an average length of ~1 μm and diameter of ~50 nm were vertically grown on the reduced graphene film surface. The crystalline structure of the ZnO NW was characterized by high resolution TEM (HRTEM) and fast Fourier transform (Fig. 3b). HRTEM analysis revealed that the synthesized ZnO NWs had a single crystalline nature and the lattice distance along the NW growth direction was 0.52 nm. The fast Fourier transform (FFT) pattern of a HRTEM image (inset in Fig. 3b) shows that the preferred NW growth direction indexed to a wurtzite structure was [0001]. Taking advantage of the high mechanical flexibility of the reduced graphene/PDMS substrate, ZnO NWs/graphene hybrids could be extremely bent without losing their structural integrity, as shown in Fig. 3c and 3d. Despite the small bending radius of ~2 mm, the structural integrity was well-maintained.

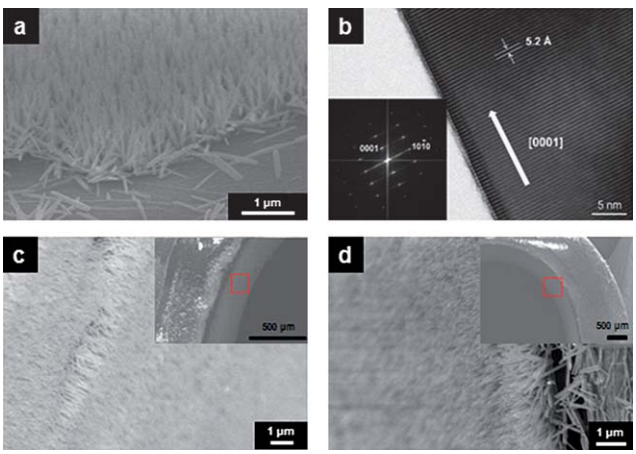

Fig. 3 (a) 60° tilted cross-sectional FE-SEM image of vertical ZnO NWs grown on the reduced graphene/PDMS substrate. (b) HRTEM image and FFT pattern (inset) showing [0001] growth direction of the ZnO NW. High- and low- (inset) magnification SEM images of high bent ZnO NWs/graphene/PDMS hybrids: (c) left-upper side and (d) right-upper side views, respectively.

Fig. 4a shows the optical transparency of PDMS, reduced graphene/PDMS, and ZnO NWs/reduced graphene/PDMS substrates, respectively. The optical transparency measured by UV-vis spectroscopy was ~70% before ZnO NW growth, which slightly decreased to ~55% after NW growth. Owing to the intrinsic transparency of ZnO with a wide band gap, the transparency decreased by only ~15%. The vertical alignment and uniform distribution of ZnO NWs also support such a high optical transparency.[29] The chemical composition of the ZnO NW was analyzed by energy dispersive X-ray spectrometry (EDS). Fig. 4b shows that the synthesized ZnO NWs are composed of zinc and oxygen (C and Cu peaks from a TEM-grid).

The work function (Φ_{ZnO}) and valence band energy of ZnO NWs were measured by ultraviolet photoelectron spectroscopy (UPS) (Fig. 5a and b). He I (21.2 eV) was utilized as a photon source for the UPS measurement, where the error margin of the obtained values was less than 1% compared to refs 30 and 33. Furthermore, the band gap of the ZnO NWs was also calculated by measuring the edge of the absorption spectrum through UV-vis spectroscopy (Fig. 5c). Based on these values of ZnO NWs, the energy-band diagram of the ZnO NWs could be estimated. The work function of the reduced graphene film ($\Phi_{\text{reduced graphene}}$) was also measured by UPS. Fig. 5d shows the work function of the reduced graphene with a value of 4.53 eV.

Fig. 6 presents a field-effect transistor (FET) test for a reduced graphene film. The metallic electro-conductivity of the reduced graphene film was confirmed by the FET test, where the source–drain current (I_{ds}) through the graphene film maintained a constant value, regardless of the gate voltage (V_g) (Fig. 6a). The inset of Fig. 6a shows a SEM image of a Pd source and drain electrodes with 80 nm thickness on the reduced graphene. The reduced graphene was patterned into 1 × 1 cm to prevent the current flow to the back gate. Fig. 6b shows a schematic

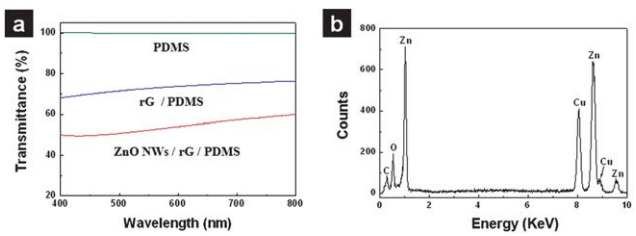

Fig. 4 (a) UV-vis spectra of raw PDMS, the reduced graphene/PDMS substrate and ZnO nanowires/reduced graphene/PDMS hybrid. (b) The TEM-EDS spectrum of the ZnO NW (C and Cu peaks from a TEM grid).

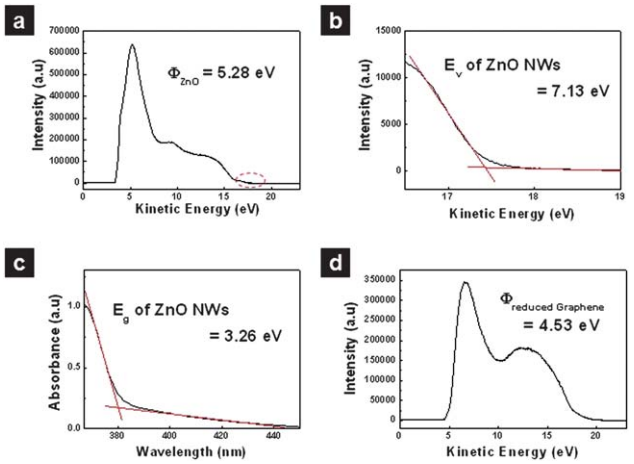

Fig. 5 (a) The ZnO nanowire work function measured using ultraviolet photoelectron spectrum (UPS). (b) The ZnO NWs valence band obtained from the magnified region of the UPS, marked with a red circle in (a). (c) ZnO nanowire band gap energy obtained from the UV-vis absorption spectrum. (d) The reduced graphene work function measured using UPS.

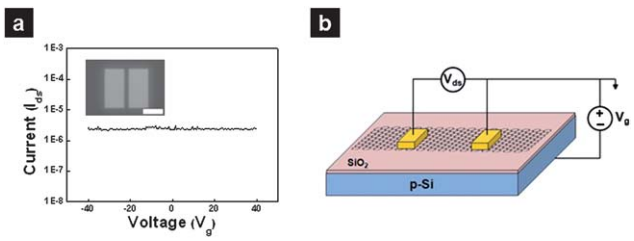

Fig. 6 (a) The I_{ds}–V_g characteristics of a reduced graphene film (film thickness: 10 nm) measured by a field-effect transistor test (inset: a SEM image of the source–drain electrodes prepared by electron beam lithography on the reduced graphene film, scale bar: 500 μm). (b) A schematic illustration of a field-effect transistor (FET) with the Pd source and drain electrodes (V_{ds} = 100 μV).

illustration of a reduced graphene FET. This device is fabricated on a boron-doped silicon substrate with 500 nm SiO_2 as the gate dielectric. The electronic measurement was carried out in ambient conditions at room temperature.

Fig. 7a shows the energy-band diagram of a ZnO NW and a reduced graphene film. The conduction band of the ZnO NWs was calculated from the difference between the measured valence band and band gap of the ZnO NWs. Fig. 7b illustrates the anticipated energy-band diagram for the direct contact of n-type semiconductor ZnO NWs with metallic reduced graphene film. To achieve thermal equilibrium in this junction with $\Phi_{ZnO} > \Phi_{reduced\ graphene}$, electrons will flow from the reduced graphene film to the ZnO NW, which renders the surface of the ZnO NW more n-type. Generally, two types of ohmic contacts are available at semiconductor–metal junctions: (i) ideal non-rectifying barriers, and ii) tunnelling barrier for a metal–heavily-doped semiconductor junction.[37] Since our ZnO NWs were undoped, we suggest an ideal non-rectifying barrier for the junction between the ZnO NWs and the reduced graphene film. The electrical contact between a vertical ZnO NW and graphene film was straightforwardly measured by EFM,[34] as shown in Fig. 7c.

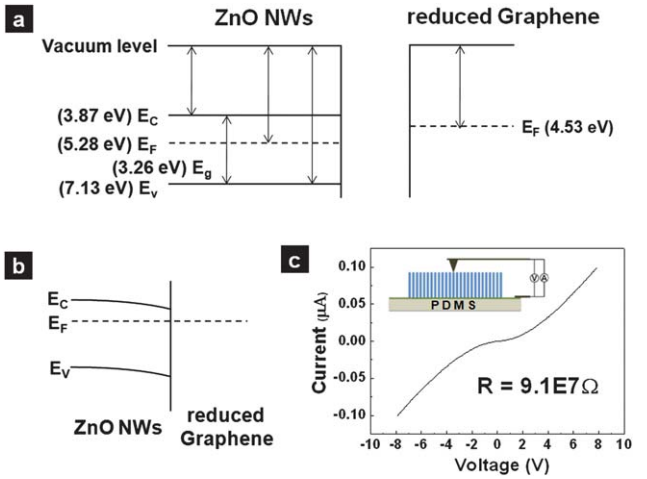

Fig. 7 (a) Energy-band diagrams of semiconducting ZnO NWs and a metallic reduced graphene film. (b) An energy-band diagram of ZnO NW–reduced graphene film junction ($\Phi_{ZnO} > \Phi_{reduced\ graphene}$). (c) An *I*–*V* plot *via* single NW and the reduced graphene layer measured by an EFM (electric force microscope).

The inset depicts the current–voltage (*I*–*V*) measurement system by EFM. Since the EFM Pt-coated cantilever tip diameter (30 nm) was smaller than the ZnO NW diameter (40–80 nm), the electric current through a vertical single NW and graphene substrate could be successfully measured as a function of the voltage. As anticipated, the obtained *I*–*V* curve exhibits typical ohmic behavior. The resistance calculated from the slope of the *I*–*V* curve was 9.1×10^7 Ω. This relatively large value is attributed to the intrinsic junction barrier between ZnO NWs and reduced graphene films, and the contact resistance at the cantilever tip/ZnO NW contact, and reduced graphene film/bottom electrode contact. Nevertheless, the smooth *I*–*V* curve with an almost linear shape represents the ohmic contact between an individual ZnO NW and the reduced graphene film substrate.

Owing to the mechanical flexibility and low contact barrier between the semiconducting NW and the metallic substrate, our ZnO NWs/graphene hybrids are potentially useful for flexible electrics and optoelectronics. As a representative example, we investigated the flexible field emission characteristics.[35,36]

Fig. 8 presents the field emission properties measured in unbent and bent states. Flexible poly(ethylene terephthalate) (PET) films sputtered with 5 nm Au were utilized as the anode for the bent ZnO NWs/graphene hybrid cathodes. Fig. 8a shows the field emission current density–applied field (*J*–*E*) curves. The turn-on field required to generate an emission current density of 10 μA cm^{-2} decreased in the order concave, flat, then convex structures. The bending radius was ~22.5 mm for both concave and convex geometries. While the turn-on voltage of a flat hybrid film was 2.4 V μm^{-1}, the turn-on field for a convex film exhibited a lower value of 2.0 V μm^{-1}. This is one of the lowest values reported for ZnO NWs field emitters.[3–6] In contrast, the concave film showed a larger value of 2.8 V μm^{-1}.

In order to get an insight into the variation of the field emission under mechanical deformation, the measured *J*–*E* curves were converted into the Fowler–Nordheim (F–N) plot ($\ln(I/V^2)$ *vs* $(1/V)$ in Fig. 8b. The plotted curves were linearly fit to calculate the

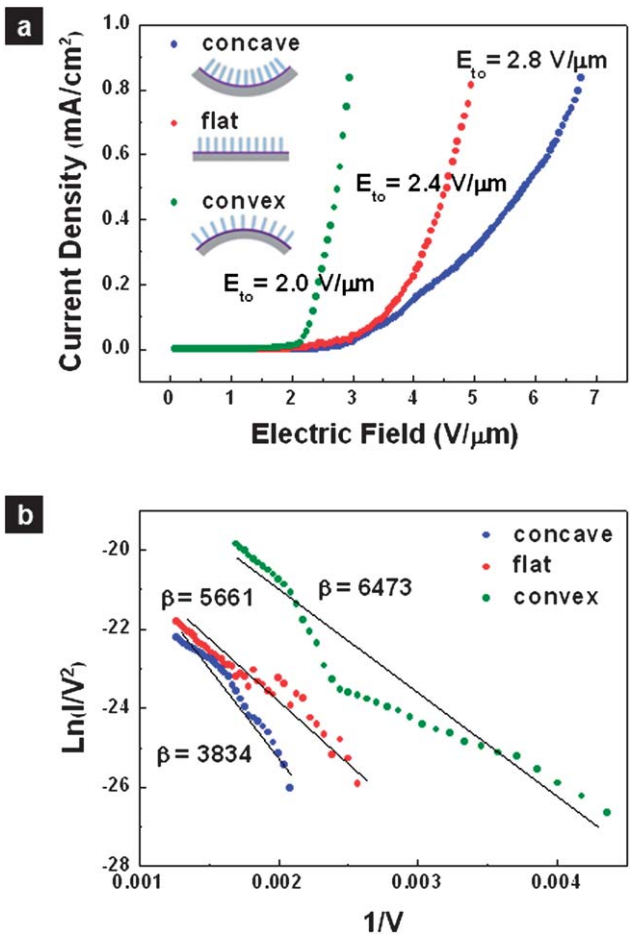

Fig. 8 The field emission properties of ZnO NWs/graphene hybrids. (a) Current density *vs* electric field curves for the bent and unbent hybrids (bending radius: 22.5 mm). (b) Fowler–Nordheim plots for the bent and unbent hybrids.

field enhancement factors (β), according to the following equation:

$$\beta = B\Phi^{3/2}d \,/\, \text{slope}, \qquad (1)$$

where Φ is the work function of ZnO, d is the distance between the anode and cathode, and $B = 6.83 \times 10^9$ $eV^{-3/2}$ V m^{-1}. The field enhancement factor (β) is generally related to the geometry, structure, and density of emitters. By taking 5.28 eV as the Φ for ZnO NWs obtained from the UPS measurement and maintaining an anode to cathode distance of 200 μm, the field enhancement factors (β) were calculated. The calculated β values were 3834, 5661, and 6473 for concave, flat, and convex films, respectively.

This large variation is attributed to the modification of the ZnO NW emitter area density upon bending. If the ZnO NWs/graphene hybrid cathode was bent inwardly, making it into a concave shape, the area density of the field emitter tips increased. This densification strengthened the screening effects from neighboring ZnO field emitters such that the overall field emitting efficiency deteriorated. Conversely, when the ZnO NWs/graphene hybrid was bent outwardly, the area density of the field emitter decreased. Under less screening from neighboring emitters, the emitting efficiency became greatly enhanced.[31,32]

Conclusions

We have demonstrated a novel transparent and flexible optoelectronic hybrid material consisting of vertically aligned ZnO NWs grown on reduced graphene/PDMS substrates. This hybrid material created from the hydrothermal synthesis of ZnO NWs on reduced graphene/PDMS substrates proved to be a promising candidate for flexible devices, such as flexible field emission devices. Owing to the good mechanical and electrical contact between vertical ZnO NWs and graphene film, the field emission of our hybrid material showed low turn-on voltages from 2.0 to 2.8 V μm^{-1}, even in highly deformed geometries. In particular, the convex bending exhibited one of the lowest values of 2.0 V μm^{-1}, due to the reduced screening effect from neighboring field emitters. We anticipate that the mechanical deformability and interesting electric and optoelectronic properties of the ZnO NWs/graphene hybrids would provide valuable insights for flexible applications, such as flexible displays and solar cells.

Acknowledgements

This work was supported by National Research Laboratory Program (R0A-2008-000-20057-0), World Class University (WCU) program (R32-2008-000-10051-0), the Pioneer Research Center Program (2009-0093758), Mid-career Research Program (2010-0015063), the National Research Foundation of Korea (NRF) grant (2008-0062204) funded by the Korea government (MEST).

References

1 M. Law, L. E. Green, J. C. Johnson, R. Saykally and P. Yang, *Nat. Mater.*, 2005, **4**, 455.
2 Z. L. Wang and J. Song, *Science*, 2006, **312**, 242.
3 Y.-K. Tseng, C.-J. Huang, H.-M. Cheng, I.-N. Lin, K.-S. Liu and I.-C. Chen, *Adv. Funct. Mater.*, 2003, **13**, 811.
4 D. Banerjee, S. H. Jo and Z. F. Ren, *Adv. Mater.*, 2004, **16**, 2028.
5 W. Wang, B. Zeng, J. Yang, B. Poudel, J. Huang, M. J. Naughton and Z. Ren, *Adv. Mater.*, 2006, **18**, 3275.
6 H. Yoon, K. Seo, H. Moon, K. S. K. Varadwaj, J. In and B. Kim, *J. Phys. Chem. C*, 2008, **112**, 9181.
7 M. H. Huang, S. Mao, H. Feick, H. Yan, Y. Y. Wu, H. Kind, E. Weber, R. Russo and P. Yang, *Science*, 2001, **292**, 1897.
8 T.-J. Kuo, C.-N. Lin, C.-L. Kuo and M. H. Huang, *Chem. Mater.*, 2007, **19**, 5143.
9 L. E. Greene, M. Law, J. Goldberger, F. Kim, J. C. Johnson, Y. Zhang, R. J. Saykally and P. Yang, *Angew. Chem., Int. Ed.*, 2003, **42**, 3031.
10 G. Xia, S.-J. Jeong, J. E. Kim, B. H. Kim, C.-M. Koo and S. O. Kim, *Nanotechnology*, 2009, **20**, 225301.
11 K. Geim and K. S. Novoselov, *Nat. Mater.*, 2007, **6**, 183.
12 K. Geim, *Science*, 2009, **324**, 1530.
13 G. Eda, G. Fanchini and M. Chhowalla, *Nat. Nanotechnol.*, 2008, **3**, 270.
14 Gómez-Navarro, M. Burghard and K. Kern, *Nano Lett.*, 2008, **8**, 2045.
15 A. Balandin, S. Ghosh, W. Bao, I. Calizo, D. Teweldebrhan, F. Miao and C. N. Lau, *Nano Lett.*, 2008, **8**, 902.
16 P. Blake, P. D. Brimicombe, R. R. Nair, T. J. Booth, D. Jiang, F. Schedin, L. A. Ponomarenko, S. V. Morozov, H. F. Gleeson, E. W. Hill, A. K. Geim and K. S. Novoselov, *Nano Lett.*, 2008, **8**, 1704.
17 J. L. Vickery, A. J. Patil and S. Mann, *Adv. Mater.*, 2009, **21**, 2180.
18 X. Wang, L. Zhi and K. Müllen, *Nano Lett.*, 2008, **8**, 323.

19 K. S. Novoselov, A. K. Geim, S. V. Morozov, D. Jiang, Y. Zhang, S. V. Dubonos, I. V. Grigorieva and A. A. Firsov, *Science*, 2004, **306**, 666.
20 K. S. Kim, Y. Zhao, H. Jang, S. Y. Lee, J. M. Kim, K. S. Kim, J. H. Ahn, P. Kim, J. Y. Choi and B. H. Hong, *Nature*, 2009, **457**, 706.
21 S. Park and R. S. Ruoff, *Nat. Nanotechnol.*, 2009, **4**, 217.
22 E.-Y. Choi, T. H. Han, J. Hong, J. E. Kim, S. H. Lee, H. W. Kim and S. O. Kim, *J. Mater. Chem.*, 2010, **20**, 1907.
23 M. B. Li, S. Muller, R. B. GiljeKaner and G. G. Wallace, *Nat. Nanotechnol.*, 2008, **3**, 101.
24 S. H. Lee, D. R. Dreyer, J. An, A. Velamakanni, R. D. Piner, S. Park, Y. Zhu, S. O. Kim, C. W. Bielawski and R. S. Ruoff, *Macromol. Rapid Commun.*, 2010, **31**, 281.
25 D. H. Lee, J. E. Kim, T. H. Han, J. W. Hwang, S. W. Jeon, S.-Y. Choi, S. H. Hong, W. J. Lee, R. S. Ruoff and S. O. Kim, *Adv. Mater.*, 2010, **22**, 1247.
26 T. H. Han, W. J. Lee, D. H. Lee, J. E. Kim, E.-Y. Choi and S. O. Kim, *Adv. Mater.*, 2010, **22**, 2060.
27 W. S. Hummers and R. E. Offeman, *J. Am. Chem. Soc.*, 1958, **80**, 1339.
28 N. I. Kovtyukhova, P. J. Ollivier, B. R. Martin, T. E. Mallouk, S. A. Chizhik, E. V. Buzaneva and A. D. Gorchinskiy, *Chem. Mater.*, 1999, **11**, 771.
29 M.-Y. Choi, D. Choi, M.-J. Jin, I. Kim, S.-H. Kim, J.-Y. Choi, S. Y. Lee, J. M. Kim and S. W. Kim, *Adv. Mater.*, 2009, **21**, 2185.
30 X. Bai, E. G. Wang, P. Gao and Z. L. Wang, *Nano Lett.*, 2003, **3**, 1147.
31 X. Wang, J. Zhou, C. Lao, J. Song, N. Xu and Z. L. Wang, *Adv. Mater.*, 2007, **19**, 1627.
32 H. Zeng, X. Xu, Y. Bando, U. K. Gautam, T. Zhai, X. Fang, B. Liu and D. Golberg, *Adv. Funct. Mater.*, 2009, **19**, 3165.
33 V. Srikant and D. R. Clarke, *J. Appl. Phys.*, 1998, **83**, 5447.
34 Y. Kim, M. Park, S. Buhlmann, S. Hong, Y. K. Kim, H. Ko, J. Kim and K. No, *J. Appl. Phys.*, 2010, **107**, 054103.
35 B. K. Lim, S. H. Lee, J. S. Park and S. O. Kim, *Macromol. Res.*, 2009, **17**, 666.
36 S. H. Lee, J. S. Park, B. K. Lim, C. B. Mo, W. J. Lee, J. M. Lee, S. H. Hong and S. O. Kim, *Soft Matter*, 2009, **5**, 2343.
37 D. A. Neamen, *Semiconductor Physics and Devices*; McGraw-Hill, New York, NY, 3rd edn, 2003.